Hindawi
Advances in Civil Engineering
Volume 2023, Article ID 5841804, 14 pages
https://doi.org/10.1155/2023/5841804

Research Article

Extrapolation-Based Scale Effect Model for Granular Heap Modulus

Zhigang Ma,[1] **Shuaifeng Wu**,[1] **and Ran Wei**[2]

[1]*State Key Laboratory of Simulation and Regulation of Water Cycle in River Basin, China Institute of Water Resources and Hydropower Research, Beijing 100048, China*
[2]*School of Transportation Science and Engineering, Beihang University, Beijing 100191, China*

Correspondence should be addressed to Shuaifeng Wu; wusf@iwhr.com

Received 19 November 2022; Revised 26 December 2022; Accepted 8 January 2023; Published 23 January 2023

Academic Editor: Bingxiang Yuan

The numerical analysis was used to predict the rockfill dam displacement, and the model parameters were calibrated using the triaxial experiments on scale-down rockfill samples. Due to the scale effect of rockfill material, the displacements were usually underestimated in the design phase. This study focused on the scale effect of rockfill material and an extrapolation model was proposed to extrapolate the prototype modulus from the laboratory modulus. By conducting confined compression experiments, the size effect was investigated using ball heaps. Based on the experimental findings, considering a granular heap as a cumulative particle structure, the structural mechanics approach was introduced to establish the size effect model. Then, the boundary constrain effect model was speculated using the elastic mechanics analysis. By conducting the confined experiments on ball heaps, the modulus variation with particle breakage was investigated and the breakage effect model was established consequently. Finally, via combining the effects from the size, boundary constrain, and particle breakage, a scale effect model was established for extrapolating prototype modulus from the laboratory modulus. The proposed model was evaluated through numerical analysis of an actual dam. The experimental results revealed that the compressive modulus decreased as the initial void ratio increased; under the same initial void ratio, the compressive modulus decreased as the ratio of the specimen width to particle size increased; the compressive modulus decreased as the particle breakage increased. The numerical analysis results showed that prediction accuracy for rockfill dam displacement was improved by 8%–10%. The proposed model represents a new approach for investigating the scale effect of rockfill material, which could be adopted by engineers to improve the prediction of rockfill dam displacement.

1. Introduction

The prediction and control of displacements is a key consideration in the design of rockfill dams. This requires not only that a proper mathematical model to be adopted for the displacement prediction but also that the parameters of this model be accurately calibrated. Theoretically, tests on the original rockfill in the field provide the best solution for calibrating such parameters for a dam. However, the original particle sizes in the field in the case of a dam with a height of more than 200 m are likely to exceed the tolerance of the test container, making it impossible to conduct tests on the original rockfill. Currently, scaling-down techniques are adopted to reduce the size of the rockfill to suit the experimental equipment [1–7]. However, it has been shown that displacements are predicted as being smaller when directly using parameters calibrated via tests on a scaled-down rockfill [8–11].

One solution is to increase the container size and build a superlarger machine. Table 1 lists some superlarge apparatuses developed by researchers. Marshal [12] conducted the triaxial experiments on EI Infiernillo dam, and Marachi [10] conducted the triaxial experiments for Oroville dam, Pyramid dam, and Crushed Basalt rockfill; they all used the apparatuses to study the rockfill shear strength, and the results showed that the inner shear angle increased as the particle size decreased. Ning and Kong [13, 14] conducted the superlarge triaxial experiments on rockfill, and the

Table 1: The super large apparatuses for rockfill triaxial experiment.

References	Specimen diameter (mm)	Specimen height (mm)	Maximum grain size (mm)	Confining pressure (MPa)	Axial load (kN)
Marshal [12]	1130	2500	180	0~2.5	0~15000
Marachi [10]	915	2286	152	0~2	0~18000
Kong et al. [13]	1000	2050	160	0~4	0~10000

results showed that the modulus calibrated by the superlarge machine was less than the modulus calibrated by the usual triaxial apparatus. Although the superlarge triaxial experiments can reduce the modulus errors between the experimental results and the actual value for prototype rockfill, the modulus value is not the real prototype value and the scale effect still exists.

The alternate solution is to determine the variation rules of the modulus with grain size so as to extrapolate the experimental modulus to the prototype modulus. Currently, the extrapolation method is more used on the shear strength extrapolation [10, 12, 15–22], and the studies on rockfill modulus are not the same as the studies on shear strength.

The variation of the modulus with the particle size has been studied by multiple researchers. Using a backtracking analysis for rockfill deformation on filling construction, Hunter and Fell [23] found that the modulus of the rockfill decreased with increasing particle diameter. Using consolidated drained triaxial tests, Varadarajan et al. [24] found that the modulus for rockfill material with rounded particles increased with increasing particle size but that angular rockfill showed the opposite trend. Using the triaxial tests, Wu et al. [25] obtained that the initial modulus of rockfill material increased as the particle size increased. The variation equations, however, were not provided in these studies.

Several extrapolation methods have been proposed. It is usually accepted that the modulus remains constant when the ratio of the specimen diameter to the particle size exceeds 6 (ASTM D4767 2011). Wang [9] proposed an empirical equation relating the experimental modulus to the in situ modulus by conducting experiments on rockfill and extrapolating the analysis to rockfill dams. Wei et al. [26] developed a multiscale unified correction model based on the contact deformation theory. These studies were presented in the plane strain space.

Although the previous studies proposed several extrapolation equations, Wang's equation is an empirical equation which lacks the theoretical proof, and Wei's equation was developed in the plane strain space which lacks the experimental evaluation. Factually, the actual rockfill tolerates the triaxial stress. So far, no extrapolation equations in the triaxial stress space were developed. To predict the actual modulus accurately, a model based on an analysis in the triaxial stress space needs to be developed and the tests on the triaxial samples need to be conducted to evaluate the model.

This study focused on the scale effect and performed an analysis in the triaxial stress space. By conducting confined compression experiments on ball heaps, the laws governing the variation of the compressive modulus according to particle size, the initial void ratio, and particle breakage were obtained, respectively, and a scale effect model is proposed to extrapolate the actual modulus from the experimental modulus of scaled-down rockfill. The proposed model was evaluated through numerical analysis for an actual rockfill dam.

2. Materials and Methods

To obtain the size effect law in which the compressive modulus varies with the particle (and specimen) size, the confined experiments were conducted on the granular heaps. To obtain the particle breakage effect law in which the compressive modulus varies with the particle breakage, the confined experiments were conducted on the ball pack cumulated by the breakable particles.

2.1. Confined Compression Experiments for the Size Effect. The confined experiments were conducted on the particle heap specimens to obtain the relationship between the compressive modulus and the size.

2.1.1. Experimental Specimen. The size effect should only consider the effect that comes from the size and avoid the impact from the breakage and particle shape. As for the experiments, the nonbroken polytetrafluoroethylene (PTFE) balls were used to configure the specimen. Balls with a diameter in the range of 10–40 mm were used (Figure 1).

The material characteristics of the balls are listed in Table 2.

The parallel scaling-down technique was used to scale the specimen. It was found that the actual dam rockfill gradation met the fractal equation [27, 28]. The fractal gradation equation is formulated as follows:

$$p_i = \left(\frac{d}{d_{\max}}\right)^{3-D} \times 100, \quad (1)$$

where d is the particle diameter, p_i is the percent of material passing the sieve ($d < d_i$), $d_{\max}$ is the maximum particle size of the specimen, and D is the fractal dimension. To model the actual dam, the fractal equation (1) was used to configure the specimen gradation. When selecting the balls to make a specimen, the maximum particle size was determined previously, and for the situation $p_i = 100\%$, it held $d \le d_{\max}$, so it was necessary to revise the definition of p_i into the mass percent with $d \le d_i$. It was also found that the D value scope of gradation is 2.2–2.63 [27], so the fractal D was used as $D = 2.5$ in this paper. In this way, the mass percent is calculated to show in Table 3. The gradation curves are as shown in Figure 2.

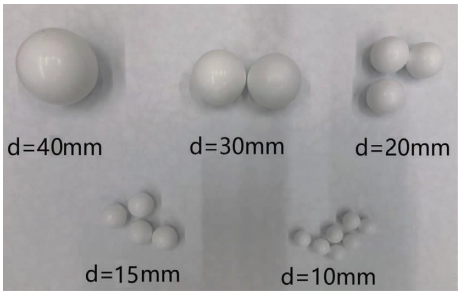

Figure 1: Balls used in tests (PTFE: polytetrafluoroethylene; d: ball diameter).

Table 2: Characteristics of particle material.

Particles	Chemical formula	Density (kg/m^3)	Young modulus (MPa)	Poisson ratio
PTFE balls	$(C_2F_4)_n$	2185.71	259.92	0.49

Table 3: Specimen gradation.

Specimen	Ball diameter, d (mm)	Mass percent, p_i (%)
Specimen with d_{max} = 40mm	40	100
	30	86.6
	20	70.7
Specimen with d_{max} = 20mm	20	100
	15	86.6
	10	70.7

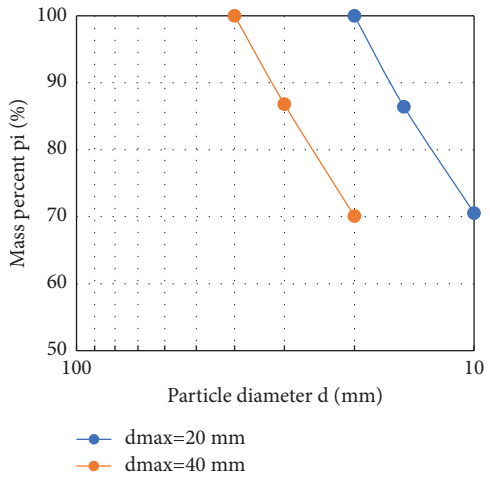

Figure 2: Gradation curves.

The balls are weighed according to Table 3 and filled into the steel container to configure the specimen, as shown in Figure 3. The containers were made into two types, one was with the inner size ($L \times B$) 120 mm × 120 mm and the other was with the inner size of 180 mm × 180 mm ($L \times B$); therefore, the specimens held the length L = 120 mm (180 mm) and the width B = 120 mm (180 mm). In this study, the void ratio of the cumulative particles was calculated as follows:

$$e_0 = \frac{L \bullet B \bullet H}{\sum_{i=1}^{n} V_i} - 1, \tag{2}$$

where V_i is the volume of ball i and n is the number of balls. In this study, the specimen depth was considered equal to the specimen width (i.e., $L = B$). From equation (2), it can be seen that the initial void ratio varies with the specimen height (H), so the specimens with various heights (H) were

Figure 3: Specimen with container.

made to get the various initial void ratio (e_0). The specimen characteristics in this study are listed in Table 4. A specimen view is shown in Figure 3.

2.1.2. Experimental Procedure. The confined compression experiments were conducted in the laboratory of the China Institute of Water Resources and Hydropower Research, in accordance with the relevant Chinese Code [1]. The testing machine was a "Universal Testing Machine Inspekt 100 kN" (Hegewald & Peschke Inc., Germany).

The experiments are conducted in accordance with the details outlined in Table 5. Meanwhile, to avoid the sidewall friction, the inner sidewalls of the steel container were skinned by the Vaseline.

2.2. Confined Compression Experiments for the Particle Breakage Effect. As a result of the breakage of grains, the rockfill compressive modulus for large angular grains is less than that for small particles [9, 24]. For purpose of investigating the particle breakage effect, the relationship between the compressive modulus and the particle breakage was tested via confined compression experiments.

2.2.1. Experimental Specimen. To examine the particle breakage, polymethylmethacrylate (PMMA) balls (Figure 4) were used to form a ball pack. The PMMA characteristics are shown in Table 6. To exclude the effects of particle sliding and to directly examine the broken particles, PMMA balls with a diameter of 10 mm were stuck to balls with a diameter of 20 mm to form a chain of balls; these chains were then placed in the experimental container in parallel to form a ball pack (Figure 4).

The geometric characteristics of the specimen are shown in Table 7.

2.2.2. Experimental Procedure. The experiments were conducted following the procedure given in Section 2.1.2 except that the maximum axial strain was setup as 20% to make the balls broken.

3. Results and Discussion

Following the experimental procedure, the confined compression experiments were conducted on the PTFE ball heaps and PMMA ball pack. The stress-strain relationship was obtained from the experiments. By analyzing the experimental data, the size effect equation which expresses the relationship between the compressive modulus and the size was obtained; also, the breakage effect equation which expresses the relationship between the compressive modulus and the particle breakage index was obtained. Based on the experimental findings, an extrapolation-based modulus model was established to extrapolate the prototype modulus from the experimental modulus.

3.1. Experimental Results. Via conducting the confined experiments on the granular heaps, the stress-strain relationship was obtained.

3.1.1. Stress-Strain Relationship for PTFE Granular Heaps. Figure 5 shows the stress-strain relationship for the PTFE ball heaps. In this paper, the ratio R_d of specimen width B to the maximum of particle diameter $d_{\max}$ ($R_d = B/d_{\max}$) was used as the size index.

3.1.2. Stress-Strain Relationship for PMMA Ball Pack. Figure 6 shows the stress-strain curve for the breakable ball pack. Note that, sharp decreases occurred at strains of 3.74%, 10.59%, and 16.7%, which means that the three balls broke at these strains. During stage I, with a strain scope of 0%–3.74%, the balls were elastically compressed and the stress-strain curve shows linear elastic behavior. Because the ball pack was nonuniform, one weak ball was broken at ε_z = 3.74%; then, the cumulative structure changed and the load was resisted by the new structure. Subsequently, the second and third balls broke; this marked stage II, with a strain scope of 3.74%–16.7%, where stress was not increasing as a result of the breakage of the particles. After the breakage was completed, the stress-strain curve entered stage III, with

Table 4: Specimen characteristics.

R_d	d_{max} (mm)	$(L \times B)$ (mm × mm)	H (mm)	e_0
3	40	120 × 120	117.93	0.670
			63.18	0.702
			45.70	0.739
			31.80	0.797
6	20	120 × 120	116.48	0.740
			88.50	0.787
			88.06	0.778
			64.35	0.833
9	20	180 × 180	119.03	0.655
			88.49	0.690
			73.995	0.699

Table 5: Experimental details.

Project	Value
Loading velocity	0.01 H/min
Preloading	1 kN
The ending of tests	One of the bellows was reached: (i) Axial strain: 5% (ii) Axial stress: 6 MPa (iii) Decrement of loading: 10%

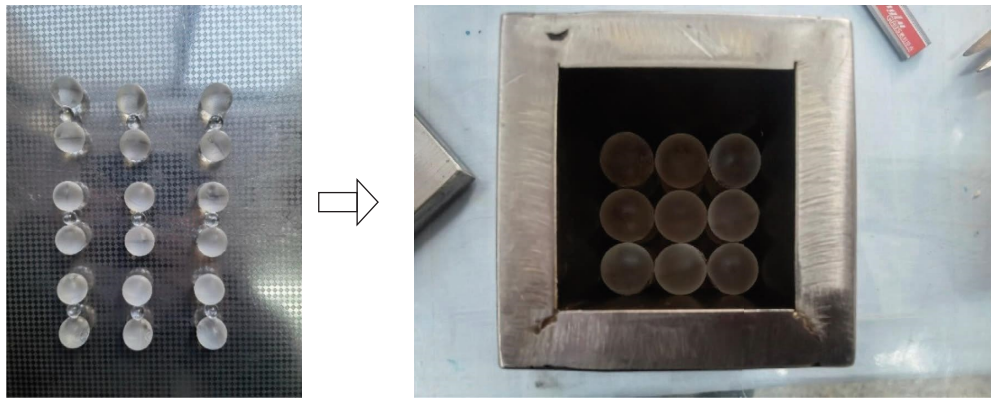

Figure 4: Pack with breakable PMMA balls.

Table 6: PMMA characteristics.

Particles	Chemical formula	Density (kg/m^3)	Young modulus (MPa)	Poisson ratio
PMMA balls	$C_{11}H_{18}O_4$	1234.43	2406.40	0.34

Table 7: Geometric characteristics of the breakable ball pack.

Width of specimen $B \times B$ (mm × mm)	Height of specimen H (mm)	Diameter of ball (mm)	Number of balls	Ball material	Initial void ratio
60 × 60	48.2	20 10	18 9	PMMA	7.94

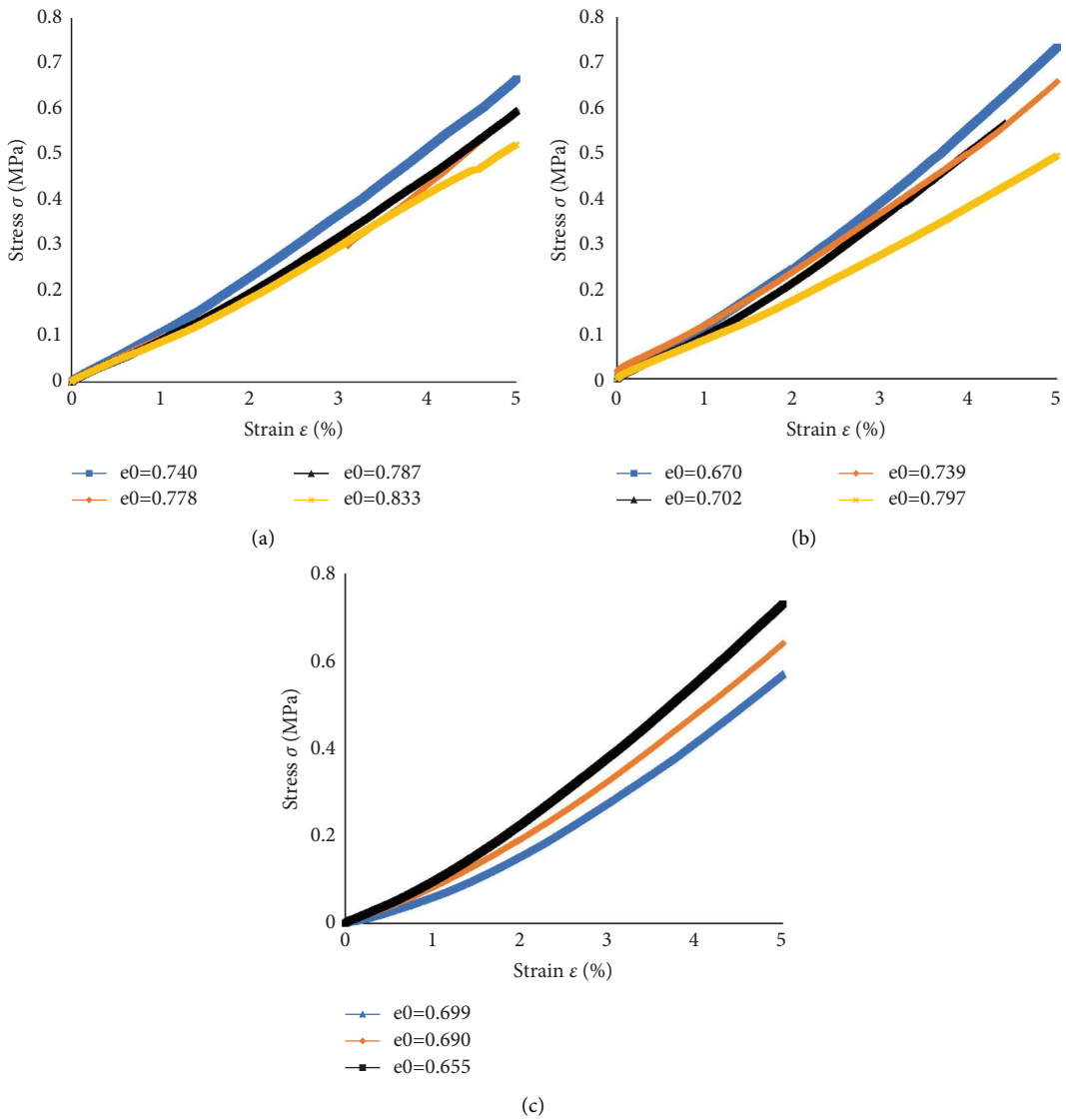

Figure 5: Stress-strain curves. (a) $R_d = 3$ ($B = 120$ mm, $d = 40$ mm). (b) $R_d = 6$ ($B = 120$ mm, $d = 20$ mm). (c) $R_d = 9$ ($B = 180$ mm, $d = 20$ mm).

a strain scope of $\varepsilon_z \geq 16.7\%$; in this stage, a stable structure once again formed to resist the load with linearly increasing stress versus strain.

3.2. Experimental Results Analysis. By analyzing the experimental results for PTFE ball heaps, the size effect equation was obtained. And, by analyzing the experimental

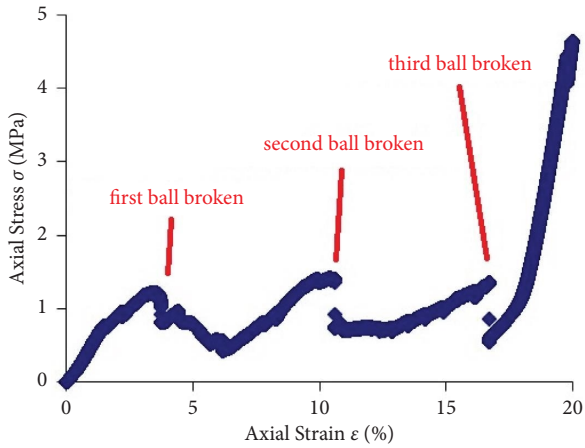

FIGURE 6: Stress-strain curve of the breakable ball pack.

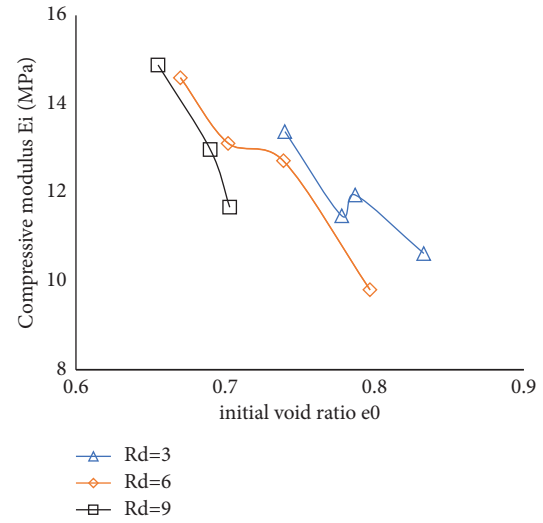

FIGURE 7: E_i–e_0 relationship for PTFE ball heaps.

results of the PMMA ball pack, the particle breakage effect equation was obtained.

3.2.1. Analysis of the Size Effect. The size effect law of granular heap was obtained by analyzing the experimental results of PTFE ball heaps. Based on the experimental findings, a size effect model was proposed adopting the structural mechanics theory. Finally, the model was assessed by the confined compression experiments.

(1) Experimental Size Effect. The compressive modulus E_i is obtained by linearly fitting the stress-strain curves in Figure 5. And, the R_d (= $B/d_{\max}$) was used as the size index. The E_i~R_d equation was obtained by fitting the experimental data.

The size effect focuses on the relationship between the compressive modulus (E_i) and the size index (R_d), which requires that the compressive modulus of the cumulative particles with various R_d should be compared under the same void ratio. As can be seen from Table 4, the same initial void ratio under different values of R_d was not obtained for the granular heap. The solution is to plot the compressive modulus (E_i) and initial void ratio (e_0) in one coordinate and to fit the data of (e_0, E_i) to obtain the E_i–e_0 equation. Then, the several equations for the various R_d can be used to calculate the compressive modulus under the same initial void ratio. The plots of (e_0, E_i) for the PTFE specimens with $R_d = 3, 6, 9$ are shown in Figure 7. Under the same R_d, the compressive modulus decreases as the initial void ratio e_0 increases, as a result, the E_i–e_0 equation can be fitted by the power function as follows:

$$E_i = \frac{\omega}{(1+e_0)^{\xi}}, \tag{3}$$

where ξ and ω are model parameters.

Also, it can be seen from Figure 7 that the E_i–e_0 curve for $R_d = 9$ locates beneath the curve for $R_d = 6$, and the curve for $R_d = 6$ locates beneath the curve of $R_d = 3$. To predict E_i, equation (3) was used. For example, selecting $e_0 = 0.70$ and 0.80, respectively, the calculated E_i and specimen R_d is plotted in one coordinate as shown in Figure 8. It can be seen that the E_i decreases as R_d increases under the same e_0, and the exponential function was used to fit data (R_d, E_i) to obtain the E_i~R_d equation as follows:

$$E_i = \lambda \bullet \exp\left(-\frac{R_d}{\eta}\right), \tag{4}$$

where λ and η are model parameters.

(2) Size Effect Model. On the basis of the results obtained from the confined compression tests, a size effect model based on the ball heap was established by analyzing the cumulative structure using the Hertz contact model in this section.

For the situation of particle-particle contact under a compressive load (Figure 9), it is assumed that the deformation is elastic, the stress occurs in the normal direction, and the contact face is squeezed to form a circular plane with radius c and the compression stresses q are distributed as an ellipsoid, which is formulated as $q = q_0\sqrt{1-(r/c)^2}$, where q_0 is the maximum stress on the contact face and r is the distance from the center ($0 < r \le c$).

On the basis of the abovementioned assumptions, Hertz formulated the following equations to relate the load to particle deformation:

$$q_0 = \frac{3P}{2\pi c^2}, \tag{5}$$

$$c^3 = \frac{3}{4}\cdot\frac{R_1\cdot R_2}{R_1+R_2}\left(\frac{1-\mu_1^2}{E_1}+\frac{1-\mu_2^2}{E_2}\right)P, \tag{6}$$

$$\delta^{\frac{3}{2}} = \frac{3}{4}\left(\frac{1-\mu_1^2}{E_1^2}+\frac{1-\mu_2^2}{E_2^2}\right)\sqrt{\frac{R_1+R_2}{R_1R_2}}P, \tag{7}$$

where δ is the compressive deformation from the center of particle 1 to the center of particle 2, E_1 and E_2 are Young's

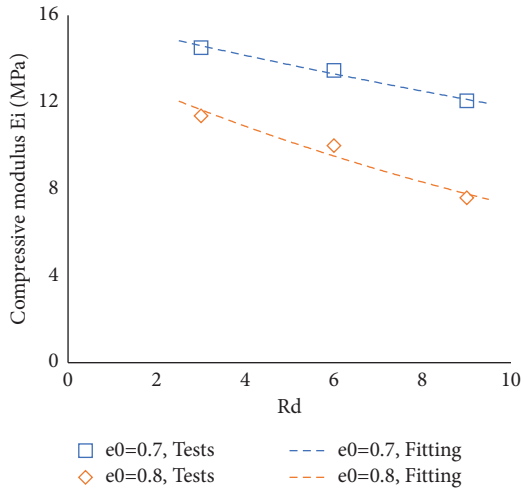

Figure 8: $E_i - R_d$ relationship for PTFE ball heaps.

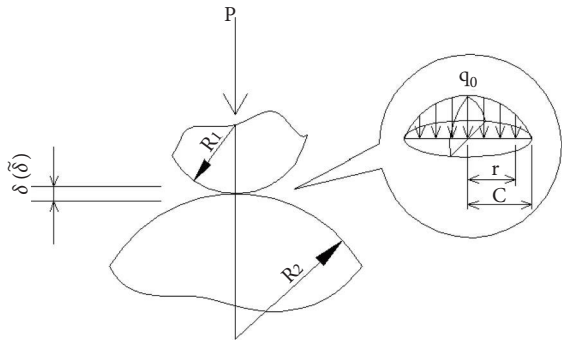

Figure 9: Contact between particles.

modulus for particles 1 and 2, respectively, and μ_1 and μ_2 are the Poisson ratios for particles 1 and 2, respectively.

Compared with equation (7), where P accords with δ as $P \propto \delta^{3/2}$ (Figure 9), the $p - \delta$ equation formulated by Hooke's law is $P \propto \delta$. The contradiction is considered to arise from the assumptions regarding the stress distributions of the ellipsoid shown in Figure 9. To eliminate the contradiction, the displacement of $\delta^{3/2}$ should be modified to satisfy Hooke's law. Hence, $\tilde{\delta}$ is defined as the displacement satisfying Hooke's law, and thus it can be easily found that $\tilde{\delta} \propto \delta^{3/2}$. Considering the size effect equation (4) derived from the experimental findings, it is assumed that the following equation holds:

$$\delta^{3/2} = a \bullet \exp\left(-\frac{R_d}{b}\right) \bullet \tilde{\delta}, \tag{8}$$

where a and b are model parameters.

For one particle inside the heap (Figure 3), while ignoring the effects of gravity acting on the particles, the forces from the adjacent particles are loaded onto the particle as shown in Figure 10.

From equation (7), the p–δ equation can be expressed as follows:

$$p = \frac{4}{3} \frac{E}{1 - \mu^2} \sqrt{R} \delta^{3/2}. \tag{9}$$

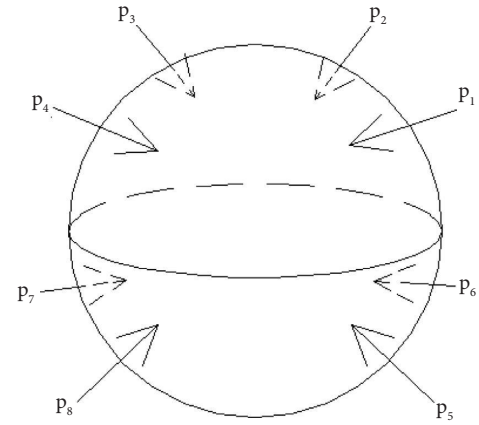

Figure 10: Forces acting on one particle.

The forces of p_i are loaded around the particle, as shown in Figure 10. Before particle breakage occurs, the ball can be considered to bear the pore pressure p and shear stress q. The pore pressure increment $\dot{p}$ can be formulated as follows:

$$\dot{p} = \frac{\sum \dot{p}_i}{n \bullet \left(4\pi R^2\right)} = \frac{1}{3\pi} \frac{E}{1 - \mu^2} \left(\frac{\dot{\delta}}{R}\right)^{3/2} = \frac{1}{3\pi} \frac{E}{1 - \mu^2} \left(\dot{\varepsilon}_v\right)^{3/2}, \tag{10}$$

where ε_v is the ball volumetric strain with $\varepsilon_v = \delta/R$.

Introducing equation (8), equation (10) is transformed into the following:

$$\dot{p} = \frac{1}{3\pi} \frac{E}{1 - \mu^2} \bullet a \exp\left(-\frac{R_d}{b}\right) \bullet \dot{\varepsilon}_v. \tag{11}$$

In this paper, the deviator strain increment $\dot{\varepsilon}_q$ was derived from the shear stress increment $\dot{q}$ and treated as the void ratio increment $\dot{\varepsilon}_q = \dot{V}_e/V$; meanwhile, the volumetric increment of the void ($\dot{V}_e$) and the volumetric increment of the particles ($\dot{V}_s$) are assumed as follows:

$$\dot{V}_e = \left[1 - (1 + e_0)^{\xi+1}\right] \dot{V}_s. \tag{12}$$

Thus, the overall strain increment $\dot{\varepsilon}$ is as follows:

$$\dot{\varepsilon} = \dot{\varepsilon}_v + \dot{\varepsilon}_q = \frac{\dot{V}_s}{(1 + e_0) V_s} - \frac{\dot{V}_e}{(1 + e_0) V_s} = (1 + e_0)^{\xi} \bullet \dot{\varepsilon}_v. \tag{13}$$

Combining equations (11) and (13), it holds the following:

$$\dot{\varepsilon} = (1 + e_0)^{\xi} \bullet \frac{\dot{p}}{(1/3\pi)\left(E/1 - \mu^2\right) \bullet a \exp\left(-R_d/b\right)}. \tag{14}$$

The forces and displacements in the heap can be obtained by integrating equation (14) to satisfy the boundary equations, as follows:

$$\iiint_V \mathrm{d}p = \iiint_V \frac{1}{3\pi} \frac{E}{1-\mu^2} \bullet a \exp\left(-\frac{R_d}{b}\right) \bullet \frac{1}{(1+e_0)^{\xi}} \mathrm{d}\varepsilon. \tag{15}$$

The boundary equations should be satisfied as follows:

Displacement boundary: $S = S_{\text{boundary}}$

Force boundary: $F = F_{\text{boundary}}$

For the confined constrains, the integration result is as follows:

$$\frac{(1+2k_0)}{3} \frac{F}{B^2} = \frac{1}{3\pi} \frac{E}{1-\mu^2} \frac{1}{(1+e_0)^{\xi}} \left[a \bullet \exp\left(-\frac{R_d}{b}\right)\right] \frac{\delta'}{H}, \tag{16}$$

where k_0 is the stress ratio of the pressure in the horizontal direction to the pressure in the vertical direction and F is the load on top of the ball heap.

Accordingly, the compressive modulus is expressed as follows:

$$E_i = \frac{1}{(1+2k_0)\pi} \left[a \bullet \exp\left(-\frac{R_d}{b}\right)\right] \frac{1}{(1+e_0)^{\xi}} \frac{E}{1-\mu^2}. \tag{17}$$

Parameter a can be obtained as follows:

$$a = \alpha B^{\beta}, \tag{18}$$

where α and β are model parameters calibrated by the test.

For a granular heap in the triaxial stress space, it is considered that the strain in the horizontal directions x and y matches the strain in the vertical direction z as follows:

$$\varepsilon_x = \varepsilon_y = -\kappa\mu\varepsilon_z, \tag{19}$$

where κ is the ratio of the horizontal strain to the vertical strain.

On the basis of Hooke's law, an equation for the coefficient of lateral pressure (k_0) can be obtained as follows:

$$k_0 = \frac{(1-\kappa)\mu}{1-\mu-2\kappa\mu^2}, \tag{20}$$

where κ is a parameter describing the deformation degree in the horizontal direction and $\kappa = 0$ for confined compression. Hence, from equation (20), it follows that the stress ratio is $k_0 = \mu/1-\mu$. Moreover, $\kappa = 1.0$ represents the unconfined compression and $k_0 = 0$. In addition, $0 < k_0 < 1.0$ means that deformation occurs in the horizontal direction.

(3) Size Effect Model Assessment. The size effect equation (17) was evaluated in this section. The confined compression tests on PTFE ball heaps were predicted using equation (17). One of the experiments was used to calibrate the parameters, and the calibrated parameters are shown in Table 8.

Using the parameters in Table 8, the modulus for experiments in Table 4 is calculated using equation (17) and the calculated E_i~e_0 curves were obtained. The E_i~e_0 curves and experimental data (e_0, E_i) are plotted in one coordinate as shown in Figure 11. It can be seen that the experimental data (e_0, E_i) locate closely to the E_i~e_0 curves and the model performance is satisfactory.

Table 8: Model parameters.

Material	α	β	b	ξ
PTFE	6.8	0.1	24	6

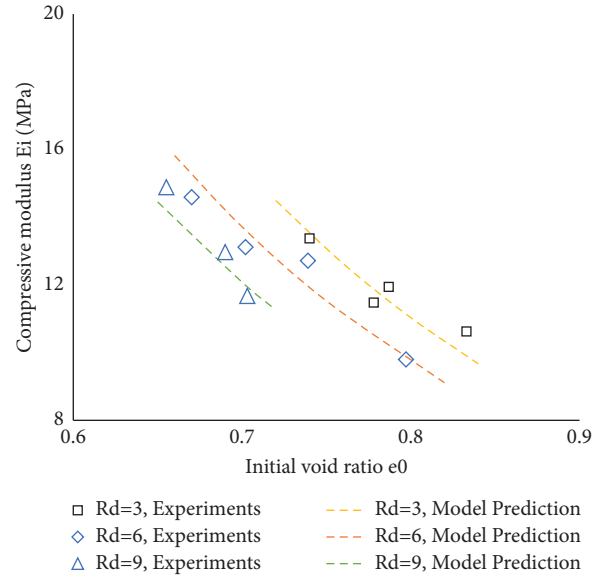

Figure 11: The calculated E_i~e_0 curves vs. the experimental data (e_0, E_i).

3.2.2. Analysis for the Particle Breakage Effect. To determine the relationship between the compressive modulus and the breakage, the experimental compressive modulus and the breakage factor should be determined from the experiment. When the confined experiment of the PMMA ball pack was finished, three balls with diameters of 10 mm were broken during the test; Figure 12 shows a view of the broken balls. As shown in Figure 6, the first ball was broken on the strain point $\varepsilon_z = 3.74\%$, the second ball was broken on the strain point $\varepsilon_z = 10.59\%$, and the third ball was broken on the strain point $\varepsilon_z = 16.7\%$. The secant modulus for the previous point of ball break of the stress-strain curve (Figure 6) is used as the compressive modulus E_i; that is, the secant modulus for the points when ε_z is equal to 3.4%, 10.36%, and 16.7%. For the purpose of analysis, the compressive modulus (E_i) is normalized by the confined compressive modulus (E_s) in the case without breakage. The normalized modulus E_i/E_s values are listed in Table 9.

As opposed to the usual breakage factor B_g [12] and B_r [29], the breakage factor used in this paper is defined as follows [30]:

$$B_v = \frac{V_b}{V_t}, \tag{21}$$

where V_b is the volume of broken balls and V_t is the total volume of the balls.

Using equation (21), the breakage factors on the previous points of ball break are calculated and listed in Table 9.

The experimental data (B_v, E_i/E_s) in Table 9 are plotted against one coordinate as shown in Figure 13, and it can be

Figure 12: Broken PMMA balls.

Table 9: Breakage factor and normalized compressive modulus.

Breakage factor B_v (%)	Normalized modulus E_i/E_s (MPa)	Strain before broken ε_z (%)
0	1.00	3.40
0.58	0.37	10.36
1.16	0.22	16.70

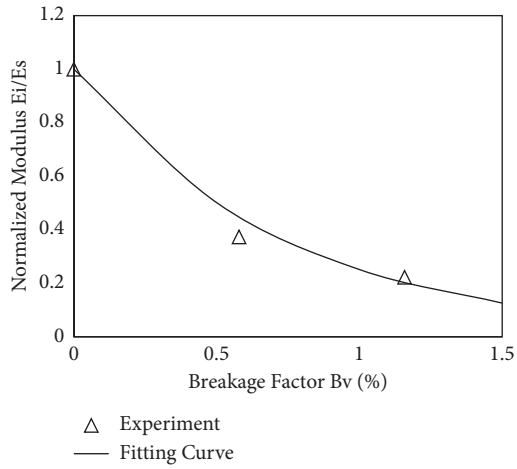

Figure 13: Plot of E_i/E_s versus B_v.

seen that the compressive modulus decreases with increasing breakage factor. Meanwhile, the exponential function was used to fit the (B_v, E_i/E_s) data to obtain the E_i/E_s-B_v equation as follows:

$$\frac{E_i}{E_s} = e^{\gamma \bullet B_v}, \tag{22}$$

where γ is the model parameter, and in this experiment, it holds $\gamma = -1.381$.

3.3. Extrapolation-Based Modulus Model. To develop a robust scale effect model for extrapolating the actual compressive modulus from a compressive modulus obtained in the laboratory, the model should account for any factor that might affect modulus extrapolation. On the basis of structural mechanics, the compressive modulus for rockfill material is determined by the cumulative structure. The structural elements are particles of several sizes and shapes, and the structural connections are the points of contact between the particles. The structural type is determined by the locations of the particles, and the structural type is randomly formed owing to the gradation and particle shape. In addition, particle breakage changes the cumulative structure during compression loading. Therefore, the compressive modulus is affected by the gradation, particle shape, the void, particle material, and particle breakage. The impact of each of these factors is considered to be simultaneous. Accordingly, an extrapolation model should comprise an equation that accounts for these factors as follows:

$$E_i = f\left(\sigma_3, D, B_v, B, d, E, \mu, e_0\right), \tag{23}$$

where E_i is the compressive modulus of particle heap, σ_3 is the lateral pressure, D is the index describing the scaling-down technique, B_v is the breakage factor, B and d are the heap width and particle diameter, respectively, E and μ are

the young modulus and Poisson ratio of particles, respectively, and e_0 is the initial void ratio.

In this paper, we assume that the modulus E_i has the following formula:

$$E_i = f(\sigma_3)\bullet f(D)\bullet f(B_v)\bullet f(B,d)\bullet f(E,\mu)\bullet f(e_0). \quad (24)$$

For extrapolating the prototype modulus from the experimental modulus, it holds the following:

$$\frac{E_s}{E_L} = \frac{f(\sigma_{3s})\bullet f(D_s)\bullet f(B_{vs})\bullet f(B_s,d_s)\bullet f(E_s,\mu_s)\bullet f(e_{0s})}{f(\sigma_{3L})\bullet f(D_L)\bullet f(B_{vL})\bullet f(B_L,d_L)\bullet f(E_L,\mu_L)\bullet f(e_{0L})}, \quad (25)$$

where subscript s means on-site and L means laboratory.

The lateral pressure effect is described as the function of lateral deformation in this paper, that is,

$$\frac{f(\sigma_{3s})}{f(\sigma_{3L})} = f(\varepsilon_x). \quad (26)$$

The size effect equation (17) was proposed basing on the confined experiments, but the actual stresses in rockfill dam are triaxial stresses, and the horizontal stresses are matching the vertical stress as

$$\sigma_x = \sigma_y = k_0\bullet\sigma_z. \quad (27)$$

Thus, the extrapolation model derived from the confined experiments should be corrected by accounting for the effect from the lateral deformation, the function $f(\varepsilon_x)$ is used here.

As can be seen from equation (19), the factor κ was introduced to describe the degree of the lateral deformation. Based on Hooke's law, the compressive modulus E_κ of a cumulative heap with horizontal deformation κ can be calculated as

$$f(\varepsilon_x) = \frac{E_\kappa}{E_s} = \frac{1-2\mu^2/(1-\mu)}{1-2\bullet(1-\kappa)\mu^2/(1-\mu)}, \quad (28)$$

where E_s is the confined compressive modulus.

The paralleled scaling method is discussed in this paper, so it holds

$$\frac{f(D_s)}{f(D_L)} = 1.0. \quad (29)$$

The breakage effect for the modulus is described as the function of the breakage factor B_v. Based on the particle breakage effect equation (22), the particle breakage effect equation $f(B_v)$ is as follows:

$$f(B_v) = \frac{f(B_{vs})}{f(B_{vL})} = e^{\gamma\bullet(B_{vs}-B_{vL})}. \quad (30)$$

The scale effect from the heap size and particle diameters is defined as the size effect in this study and described using the ratio of heap width to the particle diameter as follows:

$$R_d = \frac{B}{d}. \quad (31)$$

Therefore, the size effect for extrapolation is described as

$$\frac{f(B_s,d_s)}{f(B_L,d_L)} = f(R_d). \quad (32)$$

Based on the size effect equation (17), the function $f(R_d)$ can be described as

$$f(R_d) = \frac{1+2k_{0s}}{1+2k_{0L}}\bullet\left(\frac{B_s}{B_L}\right)^{\beta}\bullet\exp\left(\frac{R_{dL}-R_{ds}}{b}\right). \quad (33)$$

The scaling-down rockfill samples for the laboratory test are usually derived from the construction site, it holds the following:

$$\frac{f(E_s,\mu_s)}{f(E_L,\mu_L)} = 1.0. \quad (34)$$

Based on the size effect equation (17), the effect of the initial void ratio is described as

$$f(e_0) = \frac{f(e_{0s})}{f(e_{0L})} = \left(\frac{1+e_{0L}}{1+e_{0s}}\right)^{\xi}. \quad (35)$$

Combining equations (25)~(35), the scale effect model for the extrapolation is built as

$$\frac{E_s}{E_L} = f(\varepsilon_x)\bullet f(B_v)\bullet f(R_d)\bullet f(e_0). \quad (36)$$

4. Model Assessment

To evaluate model performance, an actual rockfill dam was used to predict displacements using the extrapolation model proposed in this paper. The Hekou Village dam is a concrete face rockfill dam, the geometric characteristics are as follows.

Dam height is 122.5 m, dam length is 530.0 m, top width of dam is 9.0 m, the slope for the upstream and downstream is 1 : 1.5 and 1 : 1.685, respectively, and the maximum rockfill diameter is 800 mm. Also, the rockfill characteristics are listed in Table 10.

The dam displacements were predicted using numerical analysis based on the *E-B* model in the design phase, and the model parameters were calibrated following triaxial experiments on scaled-down specimens. Meanwhile, the actual dam displacements were measured in the field during construction and throughout the operation. This study predicted dam displacement through numerical analysis using the *E-B* model with a compressive modulus modified by the proposed extrapolation model, and the results were compared to the on-site measurements and the displacements calculated from the nonmodified model.

4.1. Modeling by Using the Extrapolation Equations. Based on the method proposed in this study, the extrapolation functions were determined as follows.

The model parameters for $f(R_d)$ are listed in Table 11. Using equation (33), the value of $f(R_d)$ was $f(R_d) = 1.276$.

The model parameter for $f(B_v)$ was $\gamma = -0.031$ and breakage was $B_{vs} - B_{vL} = 15.2\%$, so the value of $f(B_v)$ was $f(B_v) = 0.625$.

Table 10: Rockfill characteristics.

Material	Dry density (g/cm^3)	Void ratio	N63.5
Alluvial subrounded rock	1.63	0.66	22

Table 11: Model parameters.

α	β	b	ξ
0.6	0.2	175	6

Table 12: Parameters of the *E-B* model.

Model	K	n	R_f	K_{ur}	c (kPa)	φ_0 (°)	$\Delta\varphi$ (°)	k_b	m
Nonmodified	1660	0.21	0.85	3320	0	54	10.6	380	0.14
Modified	1245	0.22	0.82	3320	0	54	10.6	380	0.14

Table 13: Comparison between calculated and measured dam displacement.

Type	Settlements maximum (cm)		Accuracy promotion (%)
	Construction	Water filling	
On-site measurements	78.9	109.7	
Predictions using a nonmodified model	61.2	68.1	8~10
Predictions using a modified model	69.8	77.4	

For the rockfill, the initial void ratio has the relationship with the dry density as $e_0 = G_s\rho_w/\rho_d - 1$, so the model parameter was $f(e_0) = f(\rho_d) = 1.1$.

In this paper, the value of $f(\varepsilon_x)$ was used as $f(\varepsilon_x) = 1.0$.

Using equation (36), the extrapolation modulus was $E_s/E_L = 0.877$.

For the displacement prediction, the initial compressive modulus E_i of the *E-B* model was modified. Consequently, the K and n parameters of the *E-B* model were also modified. The modified parameters were compared with the parameters obtained following triaxial experiments in the laboratory, as presented in Table 12.

4.2. Modeling Results. Numerical analysis was conducted for the dam using the software FLAC3D. The results obtained using the modified model were compared with the results calculated using a nonmodified model and on-site measurements. The comparisons are presented in Table 13. As can be seen, the modified model improved the prediction of dam displacement.

5. Conclusions

To obtain the prototype rockfill modulus, an extrapolation model was established to extrapolate the prototype modulus from the laboratory modulus. By conducting the confined tests, the variation of modulus according to the ratio of rockfill width to the particle diameter (R_d), the initial void ratio (e_0) and particle breakage was investigated, respectively. Based on the experimental results, the equations for the size effect and particle breakage effect were established. The constrain effect was speculated following the elastic mechanics theory. The main conclusions drawn from this study are as follows:

(a) Under the same R_d, the compressive modulus decreases as the initial void ratio increases. Under the same initial void ratio, the compressive modulus decreases as R_d increases

(b) The modulus decreases as the lateral deformation increases

(c) The modulus decreases as the particle breakage increases

(d) An extrapolation modulus model was established to incorporate the effect from the R_d, initial void ratio, boundary constrains, and particle breakage

The model was evaluated by the numerical analysis of an actual rockfill dam and found that the proposed model improved the prediction of rockfill dam displacement. The proposed model represents a new approach for investigating the scale effect of rockfill material, which could be adopted by engineers to improve the prediction of rockfill dam displacement.

Compared with the previous works, the extrapolation-based modulus model in this study was proposed in the triaxial stress space which matches the actual stress condition in the rockfill dam. The model was established using the structural mechanics approach, it has the theoretical basis compared with the empirical equations. However, as the cumulative particles used in this study were the balls which were different in shape to the actual rockfill material, the effect on modulus extrapolation of particle shape should be investigated in the future.

Data Availability

The data used to support the findings of this study are included within the article.

Conflicts of Interest

The authors declare that they have no conflicts of interest.

Acknowledgments

This work was supported by the Science and Technology Achievements Transformation Foundation of IWHR (Grant no. GE121003A0022022), Key Science and Technology Projects of POWERCHINA Ltd. (Grant no. DJ-ZDXM-2019-3), and National Natural Science Foundation of China (Grant no. U19A2049).

References

[1] Gb/T 50123, *Standard for geotechnical testing and method,* China Planning Press, Beijing, China, 2019.

[2] Astm D4767, *Standard Test Method for Consolidated Undrained Triaxial Compression Test for Cohesive Soils*, ASTM, West Conshohocken, PA, U.S, 2011.

[3] R. G. Hennes, "The strength of gravel in direct shear," *Direct Shear Testing of Soils*, Vol. 131, ASTM, West Conshohocken, PA, USA, 1953.

[4] J. Zeller and R. Wullimann, *The shear strength of the shell materials for the Go-Schenenalp Dam*, vol. 2, pp. 399–404, Proc 4th Inst. Jon SMFE, London, UK, 1957.

[5] J. Lowe, "Shear strength of coarse embankment dam materials," *Proceedings of the 8th International Congress on Large Dams*, vol. 3, Edinburgh, UK, 1964.

[6] E. Fumagalli, "Tests on cohesionless materials for rockfill dams," *Journal of the Soil Mechanics and Foundations Division*, vol. 95, no. 1, pp. 313–332, 1969.

[7] R. J. Frost, "Some testing experiences and character," *Evaluation of Relative Density and Its Role in Geotechnical Projects Involving Cohesionless Soils: A Symposium Presented at the Seventy-Fifth Annual Meeting, American Society for Testing and Materials*, ASTM, STP, vol. 523, p. 207, 1973.

[8] L.-S. Gao, C.-G. Cai, and J.-Q. Zhu, "An analysis method for uncoupled K-G model parameters in site confined compression test of rockfill materials and its application on CFRD," *Journal of Hydroelectric Engineering*, vol. 25, no. 6, pp. 26–33, 2006.

[9] X.-G. Wang, "Discussion on some problems observed in high earth-rockfill dams," *Chinese Journal of Geotechnical Engineering*, vol. 40, no. 2, pp. 203–222, 2018.

[10] N. D. Marachi, *Strength and Deformation Characteristics of Rockfill materials*, Department of Civil Engineering, University of California, Berkeley, CA, USA, 1969.

[11] S. Zhu, X.-P. Liang, and S.-R. Feng, "Back analysis of mechanical parameters of naturally graded rockfill materials based on large-scale loading plate tests," *Chinese Journal of Geotechnical Engineering*, vol. 31, no. 7, pp. 1138–1142, 2009.

[12] R. J. Marsal, "Large scale testing of rockfill materials," *Journal of the Soil Mechanics and Foundations Division*, vol. 93, no. 2, pp. 27–43, 1967.

[13] X.-J. Kong, J.-M. Liu, and D.-G. Zou, "Scale effect of rockfill and multiple-scale triaxial test platform [J]," *Chinese Journal of Geotechnical Engineering*, vol. 38, no. 11, pp. 1941–1947, 2016.

[14] F.-W. Ning, X.-J. Kong, D.-G. Zou, J.-M. Zou, X. Yu, and C.-G. Zhou, "Scale effect of rockfill materials and its influences on deformation and stress analysis of Aertashi CFRD," *Chinese Journal of Geotechnical Engineering*, vol. 43, no. 2, pp. 263–270, 2021.

[15] W. Hu, C. Dano, P.-Y. Hicher, J.-Y. Le Touzo, F. Derkx, and E. Merliot, "Effect of sample size on the behavior of granular materials," *Geotechnical Testing Journal*, vol. 34, no. 3, pp. 186–197, 2011.

[16] S. Linero, C. Palma, and R. Apablaza, "Geotechnical characterization of waste material in very high dumps with large scale triaxial testing," in *Proceedings of the International Symposium on Rock Slope Stability in Open Pit Mining and Civil Engineering*, pp. 59–75, Perth, Australia, September 2007.

[17] C. Ovalle, E. Frossard, C. Dano, W. Hu, S. Maiolino, and P.-Y. Hicher, "The effect of size on the strength of coarse rock aggregates and large rockfill samples through experimental data," *Acta Mechanica*, vol. 225, no. 8, pp. 2199–2216, 2014.

[18] R. Verdugo and K. De La Hoz, "Strength and stiffness of coarse granular soils," in *Soil Stress-Strain Behavior: Measurement, Modeling and Analysis*, H. I Ling and J Koseki, Eds., Springer, Netherlands, pp. 243–252, 2006.

[19] Y. Xiao, H. Liu, Y. Chen, and J. Jiang, "Strength and deformation of rockfill material based on large-scale triaxial compression tests. I: influences of density and pressure," *Journal of Geotechnical and Geoenvironmental Engineering*, vol. 140, no. 12, Article ID 04014070, 2014.

[20] M. Al-Hussaini, "Effect of particle size and strain conditions on the strength of crushed basalt," *Canadian Geotechnical Journal*, vol. 20, no. 4, pp. 706–717, 1983.

[21] B.-X. Yuan, W.-J. Chen, J. Zhao et al., "Addition of alkaline solutions and fibers for the reinforcement of kaolinite-containing granite residual soil," *Applied Clay Science*, vol. 228, Article ID 106644, 2022.

[22] B.-X. Yuan, W.-J. Chen, Z.-H. Li et al., "Sustainability of the polymer SH reinforced recycled Granite Residual Soil: properties, physicochemical mechanism and applications," *Journal of Soils and Sediments*, vol. 23, no. 1, pp. 246–262, 2022.

[23] G. Hunter and R. Fell, "Rockfill modulus and settlement of Concrete face rockfill dams," *Journal of Geotechnical and Geoenvironmental Engineering*, vol. 129, no. 10, pp. 909–917, 2003.

[24] A. Varadarajan, K. G. Sharma, K. Venkatachalam, and A. K. Gupta, "Testing and modeling two rockfill materials," *Journal of Geotechnical and Geoenvironmental Engineering*, vol. 129, no. 3, pp. 206–218, 2003.

[25] L.-Q. Wu, F. Ye, and W. Lin, "Experimental study on scale effect of mechanical properties of rockfill materials," *Chinese Journal of Geotechnical Engineering*, vol. 42, no. 2, pp. 141–145, 2020.

[26] R. Wei, S.-F Wu, X.-G. Wang, and H. Cai, "Theoretical basis and application verification of scale effects of deformation characteristics of rockfill," *Chinese Journal of Geotechnical Engineering*, vol. 42, no. 1, pp. 161–166, 2020.

[27] S. Zhu, C.-X. Zhou, X.-L. Zheng, J.-P. Gao, and Z.-G. Zhan, *Filling standards and gradation optimization of rockfill materials*, vol. 40, no. 1, pp. 108–115, 2018.
[28] Z.-Y. Chen, G.-Y. Li, K.-M. Wei, L.-Q. Wu, and Y.-M. Zhu, "Ultimate state and probability of particle breakage for rockfill materials based on fractal theory," *Chin. J. Geotech. Eng*, vol. 43, no. 7, pp. 1192–1200, 2021.
[29] B. O. Hardin, "Crushing of soil particles," *Journal of Geotechnical Engineering Journal of Geotechnical Engineering, ASCE*, vol. 111, no. 10, pp. 1177–1192, 1985.
[30] D.-Z. Kong, Q.-G. Zhang, and B.-Y. Zhang, "Particle breakage ratio of artificial rockfill materials," *Journal of Tsinghua University*, vol. 49, no. 6, pp. 796–799, 2009.